ISSN 1070-3632, Russian Journal of General Chemistry, 2015, Vol. 85, No. 10, pp. 2233–2237. © Pleiades Publishing, Ltd., 2015.
Original Russian Text © V.N. Pak, O.V. Golov, V.M. Grabov, E.V. Demidov, V.M. Stozharov, 2015, published in Zhurnal Obshchei Khimii, 2015, Vol. 85, No. 10, pp. 1600–1604.

Porous Glass as Reactor for Preparation of Bismuth Nanoparticles

V. N. Pak, O. V. Golov, V. M. Grabov, E. V. Demidov, and V. M. Stozharov

Herzen State Pedagogical University of Russia, nab. r. Moiki 48, St. Petersburg, 191186 Russia
e-mail: pakviacheslav@mail.ru

Received May 7, 2015

Abstract—Synthesis of bismuth nanoparticles in the interpenetrating channels of porous glass limiting the size of the obtained particles includes the stages of anchoring the insoluble bismuth oxide inside the glass, the oxide reduction with glycerol, and release of the metal nanoparticles from the pores volume. Hexagonal crystallites have been found in the sub-micron powder of bismuth along with its stable rhombohedral form. The prepared powders exhibited the reduced temperature and enthalpy of melting.

Keywords: porous glass, bismuth nanoparticle, crystal structure, dimensional phenomenon

DOI: 10.1134/S1070363215100035

Rapid development of methods of synthesis and study of nanosized metal bismuth are due to its potential application to the preparation of materials with enhanced thermoelectric efficiency [1–3]. Much attention has been attracted by the quantum-size metal–semiconductor transition observed for bismuth nanoparticles [3–5]. The improvement of resolution (contrast) of the X-ray images is another promising application of bismuth nanoparticles in medicine [6, 7].

Liquid-phase reduction of bismuth salts is among the chemical methods of producing its nanosized particles [5–12]; the preservation of small metal nanoparticles is a complicated problem due to the negative effect of collective recrystallization. In this regard, the reaction media should exhibit increased viscosity or incorporate certain organic additives preventing aggregation of the synthesized particles (and sometimes affecting their shape) [5–12]. Spherical and rod-like bismuth nanoparticles have been obtained via reduction of sodium bismutate at 200°C in polyethylene glycol or glycerol containing additionnally varied amounts of poly-*N*-vinylpyrrolidone, acetone, and water [12]. The high affinity of the reaction medium components to the small particles surface complicated their isolation in the pure form [5–12].

This work was inspired by the suggestion to use the interpenetrating channels of porous glass as the reaction space (nanoreactor) in order to limit the size of the synthesized bismuth particles. Glycerol could be used as the reducing agent and the medium viscosity modifier [12]. One of the synthesis schemes includes anchoring bismuth oxide inside the glass as the insoluble precursor, followed by its reduction with glycerol into metal and release of the so formed nanoparticles from the pores.

The two types of porous glass in the form of plates (membranes) with the porous structure parameters listed in Table 1 were prepared according to the procedure described in [13]. The pre-defined content of Bi_2O_3 (Table 1) at the walls of the interpenetrating channels was ensured via impregnation of the porous glass with $Bi(NO_3)_3$ aqueous solution followed by elimination of water and thermal decomposition of the salt. The yellow plates rapidly turned dark-grey upon dipping of the washed and dried porous glass–Bi_2O_3 specimens in glycerol and gradual heating to ≈200°C, thus evidencing the Bi_2O_3 reduction into the metal. Further maintaining the plates at 200°C resulted in their gradual discoloration, likely due to the spontaneous release of the metal nanoparticles into the liquid phase. Transparency of the external glycerol phase was explained by the small size and low concentration of the particles.

In order to identify the metallic nanostructures and to determine their size and shape, the bismuth–glycerol

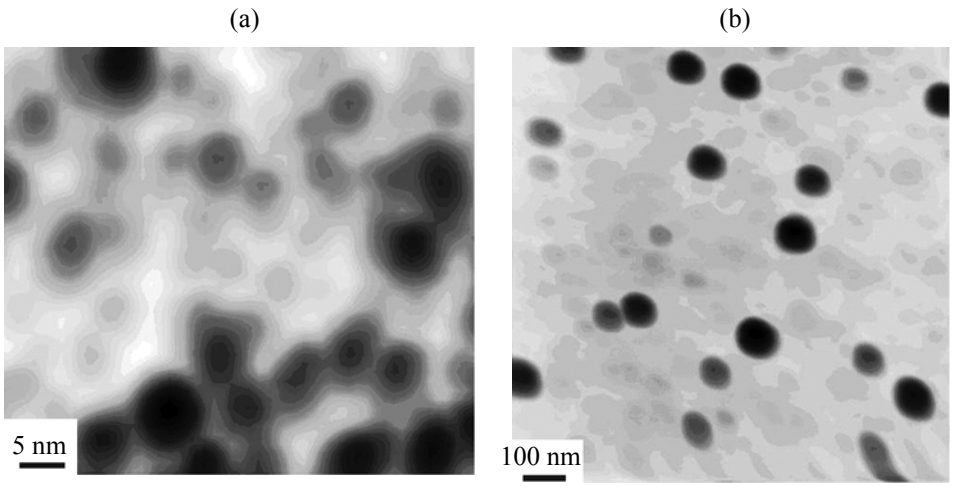

Fig. 1. Atomic force microscopy images of primary bismuth particles synthesized using porous glasses (a) **1** and (b) **2**.

colloids were applied onto an atomically smooth mica surface, heated in a vacuum at 180°C till complete evaporation of glycerol, and studied by means of atomic force microscopy. The typical images (Fig. 1) revealed the spherical shape of bismuth particles and confirmed their size limitation by the porous morphology of the nanoreactors. The particles formed in the porous glass matrix **1** with the prevailing channels diameter of 9 nm were of 5–8 nm, whereas the reduction in the larger pores (~100 nm) of glass **2** resulted in the formation of the 50–80 nm particles.

The observed displacement of the metal from the pores of the glass was evidently due to the high concentration gradient at the interphase boundary and the labile (confined) state of the solvated nanoparticles in the narrow silica channels. Displacement of the primary bismuth particles into the glycerol phase in the amounts sufficient for further examination was practically impossible due to the small size of the metal formations and high viscosity of the medium.

Accumulation of the metal particles in the liquid phase was attained by using several porous glass–Bi_2O_3 plates and longer reduction. As a result, the primary particles were united in visible aggregates that could be isolated via centrifugation. The so prepared powders were thoroughly washed with ethanol and then studied by means of atomic force and scanning electron microscopy as well as by X-ray diffraction.

Table 1. Specific surface area, pores volume, and diameter of channels in the porous glassed; content of Bi_2O_3 (Q)

Porous glass	S_{sp}, m^2/g	V_p, cm^3/g	d, nm	Q, g/g
1	80	0.16	9	0.182
2	20	0.44	100	0.196

According to the electron microscopy examination of the bismuth powder prepared using the glass **1** containing narrower pored, the spherical submicron particles prevailed (Fig. 2a). At the same time, the atomic force microscopy image of the isolated grains of the powder on mica showed that they consisted of numerous particles (subgrains) of ~10 nm (Fig. 2b). We therefore suggested that aggregation of the primary small (≈7–8 nm) bismuth particles occurred predominantly due to adhesion, the collective recrystallization being limited. The so formed grains were agglomerates of the individual particles linked together. The similar process of enlargement of the 50–70 nm particles isolated from the porous glass **2**–Bi_2O_3–glycerol system resulted in the formation of the coarse-grained bismuth powder exhibiting broad distribution of the aggregates size reaching tens of μm. Hence, the morphology of powder bismuth samples was largely determined by the size of the constituting primary particles, the latter being in turn limited by the diameter of channels in the porous glass.

The characteristic features of the bismuth samples were reflected in their crystal structure. The X-ray diffraction pattern of the coarse-grained powder (Fig. 3a) reliably confirmed the rhombohedral bismuth structure, other reflections being absent [1–6]. Hence, the metal particles were highly pure and, consequently, stable against oxidation under conditions of the experiment. The high intensity of the reflections at 2θ = 27.11°, 37.89°, and 39.55° pointed at the

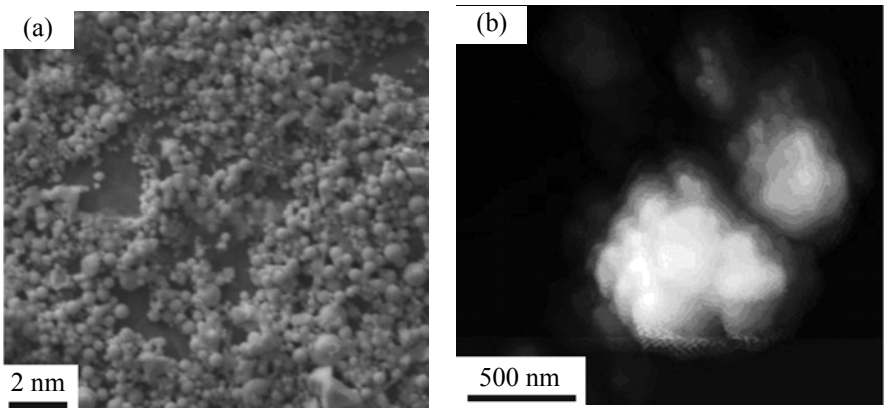

Fig. 2. (a) Scanning electron microscopy and (b) atomic force microscopy images representing the result of aggregation of primary bismuth nanoparticles shown in Fig. 1a.

predominant orientation of the crystallite along their [012], [104], and [110] planes.

The bismuth powder prepared using the porous glass **1** revealed the complex X-ray diffraction pattern. The peaks characteristic of the rhombohedral structure were accompanied by six additional reflections (Fig. 3b, Table 2). The dominating strong major peak ($2\theta = 10.80°$) left out the possible assignment of the additional pattern to bismuth oxide or high-pressure bismuth modifications. The small angle corresponding to the basic reflection suggested the presence of the hexagonal structure, its features being expressed by Eq. (1) [14]:

$$\sin^2\theta_{hkl} = A(h^2 + hk + k^2) + Cl^2, \quad (1)$$

with $A = \lambda^2/3a^2$; $C = \lambda^2/4c^2$; *hkl*, the Miller indices of the crystallographic planes; $\lambda(\mathrm{Cu}K_\alpha) = 1.5406$ Å; *a* and *c*, the lattice constants. Solution of Eq. (1) for the corresponding reflections (Table 2) gave the following parameters: $A = 8.859 \times 10^{-3}$, $C = 3.222 \times 10^{-3}$, $a = 9.450$ Å, and $c = 13.570$ Å. Validity of the identification was confirmed by the close values of the interlayer distances (Table 2) determined from the peaks positions in the X-ray diffraction curve ($d_{exp} = \lambda/2\sin\theta$) and those calculated using the quadratic Eq. (2) for hexagonal structure [14].

$$1/d^2_{calc} = 4(h^2 + hk + k^2)/3a^2 + l^2/c^2, \quad (2)$$

A special feature of the phase characterized with the indices was the *c*/*a* ratio of 1.436, noticeably smaller than that for ideal hexagonal packing (1.633 [14]). That deviation marked the decreased distance between the bismuth layers in the primary nanoparticles formed in the confined reaction volume. Hence, the influence of the narrow channels of porous glass **1** was reflected in both the size and the structural features of bismuth nanoparticles. The fraction of the hexagonal phase determined from the ratio of the total intensities of the reflections (Fig. 3b) was about 35%.

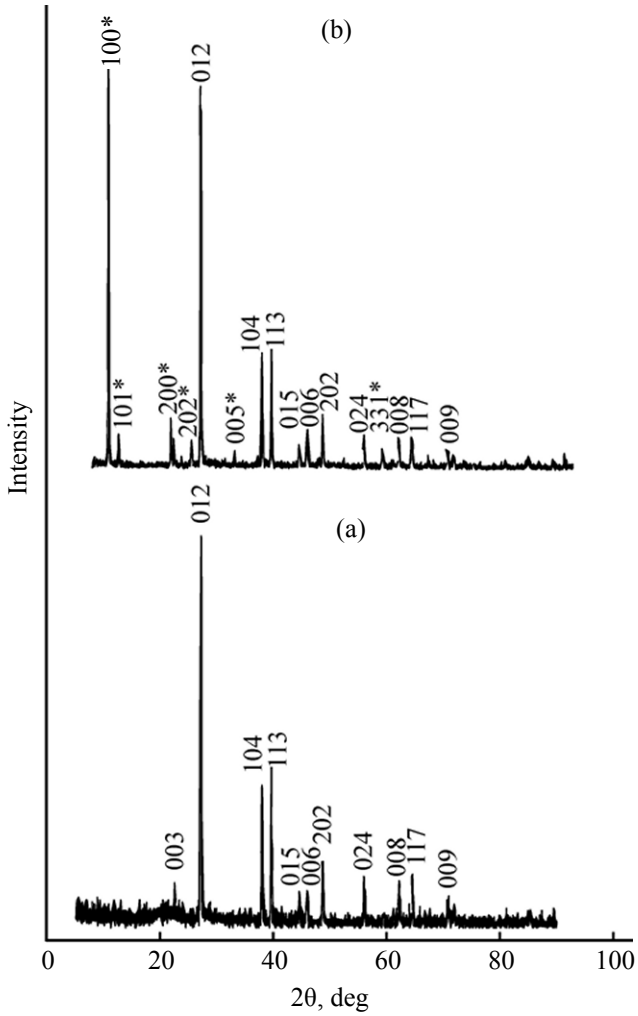

Fig. 3. X-ray diffraction patterns of bismuth powders prepared using porous glasses (a) **2** and (b) **1**.

Table 2. Comparison of experimental and calculated interlayer spacing of hexagonal structure of bismuth nanoparticles

Run no.	2θ, deg	*I*, rel. units	*hkl*	d_{exp}, Å	d_{calc}, Å
1	10.8028	320.2	100	8.1831	8.1841
2	12.6193	7.4	101	7.0090	7.0083
3	21.8171	20.0	200	4.0704	4.0920
4	25.4422	3.7	202	3.4981	3.5041
5	33.0735	3.1	005	2.7063	2.7141
6	59.3465	2.6	331	1.5560	1.5645

The known fact that the nanosized forms of metals melt at lower temperature than the bulk phase [15], was confirmed by the study of the prepared bismuth powders. Contrary to the expectations, the two samples revealed only slight difference between the melting points. The thermograms of the fine- and coarse-grained bismuth powders showed practically the same melting onsets (265.1±0.4°C), significantly lower as compared to the crystalline bismuth powder (270±0.2°C). The broadened DTA curves of the prepared samples could be due to the sintering of the nanoparticles constituting the grains preceding the grains melting. The most prominent difference was revealed for the melting enthalpies calculated from the peak areas with respect to the powder mass. The nanosized bismuth forms exhibited the close values of ΔH_m = 5.6±0.5 kJ/mol, twice lower as compared to their polycrystalline analog (11.2±0.3 kJ/mol).

The dimensional effect on the melting behavior of the samples was fairly distinct; however, the numerical values of the melting point and enthalpy should be carefully examined. Their deviation from the corresponding reference data for the bulk bismuth (271.4°C and 11.05 kJ/mol [16]) could be caused by the quality of the used specimen, its dispersity, apparent density, and distribution of the particles. As expected, X-ray diffraction patterns of the specimens after melting contained exclusively the reflections corresponding to the rhombohedral metal structure.

EXPERIMENTAL

The prepared bismuth samples were analyzed using the equipment installed at Center for Joint Usage, Herzen State Pedagogical University of Russia.

The bismuth nanoparticles were visualized using a Solver P-47 atomic force microscope and a Zeiss EVO-40 scanning electron microscope. X-ray diffraction patterns were registered using a Dron-7 diffractometer equipped with copper anode. Differential thermal analysis was performed using an STA 449 F3 Jupiter instrument.

Parameters of porous structure of the used glass plates **1** and **2** are collected in Table 1.

Bismuth oxide Bi_2O_3 was prepared as follows. The porous glass was soaked with 2.0 mol/L aqueous solution of $Bi(NO_3)_3$; the samples were first dehydrated at 120°C, and then the incorporated salt was completely decomposed via annealing at 500°C in air. The formation of the Bi_2O_3 oxide in the porous glass was monitored by weighing (Table 1). In order to keep the oxide amount constant for both glasses, the above-described modification of the glass **1** with the lower pores volume was repeated three times. The pores were then filled with the reducing agent (glycerol) as follows. First, glycerol rose via the capillaries from one of the planar surfaces of the sample, the air being released from the pores on the opposite surface. The plates were then dipped in the beaker filled with glycerol, and the mixture was heated at 200°C. The reaction course (reduction of the oxide particles and release of the products) was monitored visually, observing the modified glass plates discoloration.

ACKNOWLEDGMENTS

This work was financially supported by the Ministry of Education and Science of Russian Federation in the frame of the basic part of the governmental contract.

REFERENCES

1. Lin, Y.-M., Sun, X., and Dresselhaus, M.S., *Phys. Rev. (B)*, 2000, vol. 62, no. 7, p. 4610. DOI: 10.1103/PhysRevB.62.4610.
2. Heremans, J.P., Thrush, C.M., Morelli, D.T., and Wu, M.-C., *Phys. Rev. Lett*., 2002, vol. 88, no. 21, p. 216801. DOI: 10.1103/PhysRevLett.88.216801.
3. Wang, Y.W., Kim, J.S., Kim, J.H., and Kim, K.S., *Appl. Phys. Lett*., 2006, vol. 88, no. 14, p. 143106. DOI: 10.1063/1.2192624.
4. Rasche, B., Seifert, G., and Enyashin, A., *J. Phys. Chem. (C)*, 2010, vol. 114, no. 50, p. 22092. DOI: 10.1021/jp1081565.
5. Brown, A. and Goforth, A.M., *Chem. Mater*., 2012, vol. 24, no. 9, p. 1599. DOI: 10.1021/cm300083j.
6. Pan, D., Roessl, E., Schlomka, J., Caruthers, S.D., Senpan, A., Scott, M.J., Allen, J.S., Zhang, H., Hu, G., Gaffney, P.J., Choi, E.T., Rasche, V., Wickline, S.A.,

Proksa, R., and Lanza, G.M., *Angew. Chem*., 2010, vol. 49, no. 50, p. 9635. DOI: 10.1002/anie.201005657.

7. Boldt, R., Kaiser, M., Ko'hler, D., Krumeich, F., and Ruck, M., *Nanolett.,* 2010, vol. 10, no. 2, p. 208. DOI: 10.1021/nl903291j.
8. Velasco-Arias, D., Zumeta-Dube, I., Diaz, D., and Santiago-Jasinto, P., *J. Phys. Chem. (C)*, 2012, vol. 116, no. 27, p. 14717. DOI: 10.1021/jp304170k.
9. Derrouiche, S., Loebick, C.Z., and Pfefferle, L., *J. Phys. Chem. (C)*, 2010, vol. 114, no. 8, p. 3431. DOI: 10.1021/jp9109354.
10. Xia, F., Xu, X., Li, X., Zhang, L., Zhang, L.-I., Qiu, H., and Wang, W., *Ind. Eng. Chem. Res*., 2014, vol. 53, no. 26, p. 10576. DOI: 10.1021/ie501142a.
11. Wang, Z., Jiang, C., Huang, R., Peng, H., and Tang, X., *J. Phys. Chem. (C)*, 2014, vol. 118, no. 2, p. 1155. DOI: 10.1021/jp4065505.
12. Wang, J., Wang, X., Peng, Q., and Li, Y., *Inorg. Chem*., 2004, vol. 43, no. 23, p. 7552. DOI: 10.1021/ic049129q.
13. Lyubavin, M.V., Burkat, T.M., and Pak, V.N., *Inorg. Mater.,* 2008, vol. 44, no. 2, p. 203. DOI: 10.1134/S0020168508020222.
14. Mirkin, L.I., *Rentgenostrukturnyi analiz. Inditsirovanie rentgenogramm* (X-ray Analysis. The Indexing of Radiographs), Moscow: Nauka, 1981, p. 384.
15. Niu, K.Y., Park, J., Haimei Zheng, H., and Alivisatos, A.P., *Nanolett*., 2013, vol. 13, no. 10, p. 5715 DOI: 10.1021/nl4035362.
16. Rabinovich, V.A. and Khavin, Z.Ya., *Kratkii khimicheskii spravochnik* (A Brief Chemical Handbook), Leningrad: Khimiya, 1977, p. 58.